Available online at www.sciencedirect.com
ScienceDirect
International Journal of Heat and Mass Transfer 49 (2006) 5049–5061
International Journal of HEAT and MASS TRANSFER
www.elsevier.com/locate/ijhmt

Simultaneous measurement of local film thickness and temperature distribution in wavy liquid films using a luminescence technique

A. Schagen [a], M. Modigell [a,*], G. Dietze [b], R. Kneer [b]

[a] Department of Chemical Engineering, Chair of Mechanical Unit Operations, RWTH Aachen University, Germany
[b] Institute of Heat and Mass Transfer, Faculty of Mechanical Engineering, RWTH Aachen University, Germany

Received 25 April 2006
Available online 22 August 2006

Abstract

Heat transfer in falling liquid film systems is enhanced by waviness. Comprehension of the underlying kinetic phenomena requires experimental data of the temperature field with high spatiotemporal resolution. Therefore a non-invasive measuring method based on luminescence indicators is developed. It is used to determine the temperature distribution and the local film thickness simultaneously. First results are presented for the temperature distribution measurement in a laminar-wavy water film with a liquid side Reynolds number of 126 flowing down a heated plane with an inclination angle of 2°. The measured temperature distributions are used to calculate the local heat transfer coefficient and the convective heat flux perpendicular to the wall for different points in the development of a solitary wave.

Keywords: Falling film; Wave induced enhancement of heat transfer; Local heat transfer coefficient; Effective heat flux

1. Introduction

The liquid phase in applications of chemical and life science industry, like film evaporators, absorption heat pumps and falling film reactors, often occurs as gravity driven flow in form of thin liquid films. It is observed that heat and mass transfer in wavy film flow is significantly higher than in a smooth film. A variety of investigations have been performed to analyze heat and mass transfer resulting in semi-empirical correlations to describe transfer enhancement in such film systems, see Brauner and Maron [10], Wasden and Dukler [29], Conslisk [12], Alekseenko et al. [3], Alhusseini et al. [2], Roberts and Chang [22] and Miladinova et al. [18]. For a critical review of models of coupled heat and mass transfer in falling film absorption see Killion and Garimella [15]. The mechanisms of transport processes leading to the enhancement of heat transfer in such systems are not clarified in detail. Because of the complexity of the system it is not possible to identify the responsible transport mechanism from integral measurements of heat transport.

To analyze these phenomena in detail, heat transfer in falling liquid films is investigated in the Collaborative Research Center (SFB) 540 "Model-based Experimental Analysis of Kinetic Phenomena in Multi-phase Fluid Reactive Systems". To gain deeper insight two essential objectives were pursued: to identify the precise hydrodynamic regime in falling liquid films and to obtain highly resolved experimental data on the temperature distribution in a heated film.

The small film thickness requires a non-invasive measuring method to avoid disturbance of the film. There exist some well developed non-invasive optical measurement techniques e.g. laser doppler anemometry (LDA) and particle image velocimetry (PIV) for velocity field measurement. Measurements of the velocity field in wavy film flow were performed by Al-Sibai et al. [7]. For information about local film thickness a chromatic confocal imaging method can be used, see Lel et al. [16]. For temperature

* Corresponding author. Tel.: +49 241 80 95159; fax: +49 241 80 92252.
E-mail address: modigell@ivt.rwth-aachen.de (M. Modigell).

0017-9310/$ - see front matter © 2006 Elsevier Ltd. All rights reserved.
doi:10.1016/j.ijheatmasstransfer.2006.06.010

Nomenclature

c	specific heat capacity, J/(kg K)
C	molar concentration, mol/m^3
c_w	wave peak velocity, m/s
d	thickness, diameter, m
F	generalized flux, 1/s
f	frequency, 1/s
H	height of channel, m
I	intensity, W/m^2
K	constant device factor, V m/W
k	wave number $= 2\pi/\lambda$, m^{-1}
L	length of channel, m
M	measured phosphorescence, V
n	distribution of effective emission area, m^2
N	number of nodal points
Pr	Prandtl number $= \nu/\kappa$
q	heat flux, J
Re	Reynolds number $= \dot{V}/(\nu\ W)$
t	time, s
u	streamwise velocity, m/s
V	volume, m^3
v	transversal velocity, m/s
W	width of channel, m
x	streamwise coordinate, m
y	normal coordinate, m

Greek symbols

α	heat transfer coefficient, W/(m^2 K)
ε	relative deviation, bound
γ	parameter
η	dynamic viscosity, kg/(m s)
φ	inclination angle, °
κ	thermal diffusivity, m^2/s
λ	thermal conductivity, W/(m K)
λ	wave length, m
ν	kinematic viscosity, m^2/s
ϑ	temperature, °C
ρ	density, kg/m^3
τ	decay constant, s
ξ	non-dimensional normal coordinate

Subscripts

0	initial or reference value
d	disturbance
diff	diffusional
eff	effective
exp	experimental
f	film
g	gas
i	interface
l	liquid, lower bound
m	mean
ob	observation volume
sta	stagnant liquid
u	upper bound
w	wave, wall

field measurements thermo-chromic liquid crystals (TLC) were used. For example, Günther and Rudolf von Rohr [23,24] measured temperature and velocity fields in turbulent natural convection by combining PIV and liquid crystal thermography (LCT). Temperature field measurements of thermal convection from a heated horizontal surface applying two-color laser induced fluorescence (LIF) were performed by Sakakibara and Adrian [26]. In order to get field information about velocity and temperature simultaneously a combination of PIV and planar laser induced fluorescence (PLIF) is used. Hishida and Sakakibara [14] used this method to investigate impinging jets. In the cases where PLIF is used to get information about the temperature distribution, the region of interest has to be optically accessible in two perpendicular planes to realize the planar laser sheet and to measure the emission of the excited indicator. This results in certain geometrical restrictions for the systems to be investigated.

The proposed optical method presented in this paper makes use of optical probes which allow to provide the temperature distribution in a film flowing down a heated plane and the local film thickness simultaneously in both high spatial and high temporal resolution. The measurements are possible at several user-defined points of interest at the same time. The data obtained from the presented measurements is used to determine the local heat transfer coefficients in a single wave. To quantify the effect of the wave induced convective transport on the heat transfer in the wavy film flow an effective heat flux is introduced and evaluated using the experimental data.

2. Physical basics

For the investigation of the heat transport in a laminar-wavy liquid film of water the optical indicator biacetyl (2,3-butanedione) is used. Biacetyl has a molar mass of 86.09 g/mol and a density of 0.99 g/cm^3 (20 °C). It emits phosphorescence as well as fluorescence when illuminated with UV-light. In an aqueous solution the phosphorescence and fluorescence intensity depend on temperature and indicator concentration. Furthermore the phosphorescence is quenched by dissolved oxygen in the water whereas the intensity of fluorescence is independent of oxygen. The latter interrelationship was used to measure concentration distributions C of absorbed oxygen in laminar-wavy liquid films, see Schagen and Modigell [27].

After a pulsed excitation with UV-light the phosphorescence emission I decreases with time according to

$$I(C,\vartheta,t) = I_0(C,\vartheta)\mathrm{e}^{-t/\tau(C,\vartheta)}. \quad (1)$$

In this equation I_0 is the initial emission intensity after turning off the excitation and τ is the decay constant of the phosphorescence emission.

In this work only oxygen free aqueous solution ($C = 0$) is used and so the phosphorescence emission depends only on temperature. Measurements have been performed to analyze the correlation between the temperature and the decay constant of the phosphorescence emission using the optical device described in Section 4.1. A tempered glass vessel, equipped with a thermocouple and a magnetic stirrer, was filled with 1 l of demineralized water, which was stripped of dissolved oxygen with purified nitrogen bubbles. After the degasification the luminescence indicator biacetyl was added in a concentration of 11.4 mol/m^3. This biacetyl concentration was used by Bäckström and Sandros [11] in their experiments to determine the decay constant of the phosphorescence emission. The concentration of biacetyl is very low compared to the solubility concentration of 285 mol/m^3 to prevent self quenching of the emission. The temperature dependency of the phosphorescence decay constant was measured in the range from 10 to 30 °C as depicted in Fig. 1.

The experimental data can be approximated with the linear equation

$$\tau(\vartheta) = -3.4\times10^{-6}\ \mathrm{s/^\circ C}\cdot\vartheta + 2.99\times10^{-4}\ \mathrm{s} \quad (2)$$

with a residual norm of 2.94×10^{-6} and a mean standard deviation of 2.3×10^{-5} s. The measurement at $\vartheta = 20$ °C is in good agreement with the value of Bäckström and Sandros [11] who reported a value of $\tau = 229$ μs. The measurement of Almgren [5] of 201 μs at 25 °C was obtained with a higher concentration of biacetyl in aqueous solution which possibly caused self quenching of the phosphorescence emission.

By measuring the decay of the phosphorescence in an isothermal system of aqueous biacetyl solution the temperature can be simply determined. Describing the measured data by

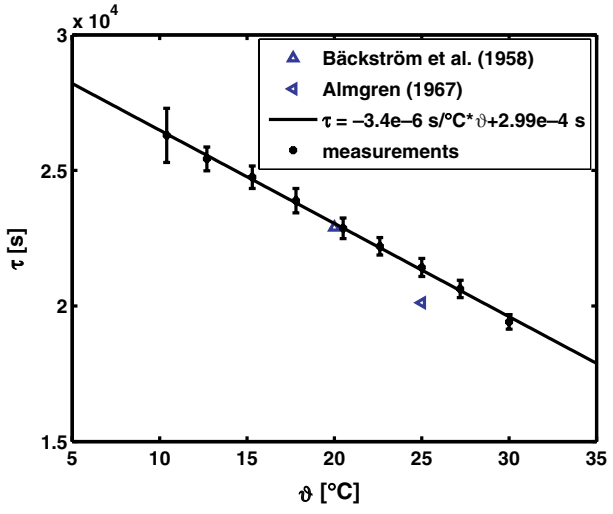

Fig. 1. Decay constant of biacetyl phosphorescence in an oxygen free aqueous solution depending on temperature.

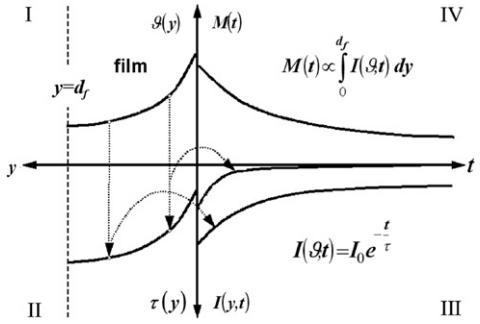

Fig. 2. Dependence of measured signal $M(t)$ on temperature profile $\vartheta(y)$ in a stagnant liquid film.

applying Eq. (1) the decay constant τ is obtained. Finally, making use of Eq. (2), the temperature can be calculated.

In case of a non-uniform temperature distribution in a stagnant liquid film every volume element emits a specific phosphorescence after excitation, depending on the local temperature, as sketched in Fig. 2.

In quadrant I a temperature profile in a liquid film is qualitatively shown as a function of the coordinate y, which is oriented perpendicular to the surface of the film. The surface of the film is indicated by d_f. Quadrant II shows the corresponding course of the local decay constant also as a function of y. The local initial intensity and the respective time dependent specific phosphorescence intensity emitted from two locations in the film, indicated with the arrows, are drawn in quadrant III. The phosphorescence totally emitted by all volume elements along the coordinate y is given by the integral equation

$$M_{\mathrm{sta}}(t) = K\int_0^{d_f} I(\vartheta,t)\,\mathrm{d}y \quad (3)$$

as indicated in quadrant IV in Fig. 2. The factor K in Eq. (3) contains apparatus and device specific contributions to the optical signal which can be assumed to be constant.

Decay constant and initial intensity of the phosphorescence change with temperature and are related to each other

$$\frac{I_0(\vartheta)}{I_0(\vartheta_0)} = \frac{\tau(\vartheta)}{\tau(\vartheta_0)}. \quad (4)$$

Herein τ and I_0 are the decay constant and the initial intensity of the phosphorescence for a solution at the variable temperature ϑ and the reference temperature ϑ_0.

Finally, the total intensity M emitted by the observation volume in a flowing liquid film is influenced by the velocity distribution $u(y)$. During the measurement volume elements containing excited biacetyl molecules move out of the fixed observation volume due to their local velocities. The resulting superposed decrease of the measured signal can be modelled based on the residence time of excited biacetyl molecules within the observation volume. This leads to

$$M(t) = K\int_0^{d_f} n_I(y,t)I(\vartheta,t)\,\mathrm{d}y, \quad (5)$$

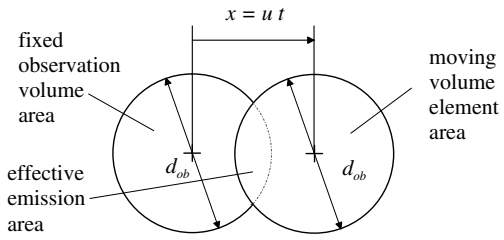

Fig. 3. Effective emission area of a volume element within the moving liquid film.

where n_I is the distribution of the luminescent area within the cross section of the measurement volume, see Fig. 3, and can be modelled as

$$n_I(y,t) = \frac{2}{\pi}\left[\arccos\left(\frac{u(y)t}{d_{\mathrm{ob}}}\right) - \frac{u(y)t}{d_{\mathrm{ob}}^2}\left(d_{\mathrm{ob}}^2 - (u(y)t)^2\right)^{1/2}\right] \tag{6}$$

using basic geometrical relations.

The exact velocity field in our experiment is unknown. Yet the velocity distribution in flow direction $u(y)$ in wavy films can be approximated by a parabolic profile

$$u(y) = u_{\max}\left[2\frac{y}{d_{\mathrm{f}}} - \left(\frac{y}{d_{\mathrm{f}}}\right)^2\right] \tag{7}$$

comparable to the analytical solution of Nusselt [19]. Here the parameter $u_{\max}$ is the longitudinal component of the local surface velocity, see e.g. Alekseenko et al. [4] and Al-Sibai et al. [7]. Based on experimental investigations on film flow of Adomeit et al. [1] and Al-Sibai et al. [7] we propose a linear interpolation of the surface velocity within the film thickness region $d_{\mathrm{f},m} < d_{\mathrm{f}} < d_{\mathrm{f,max}}$. Thus the longitudinal surface velocity component can be calculated:

for $d_{\mathrm{f}} \leqslant d_{\mathrm{f},m}$:
$u_{\max} = u_{\max,Nu} = \frac{g\sin\varphi}{\nu} d_{\mathrm{f}}^2$
for $d_{\mathrm{f},m} < d_{\mathrm{f}} < d_{\mathrm{f,max}}$:
$u_{\max} = u_{\max,Nu} + (u_{\mathrm{w}} - u_{\max,Nu})\frac{d_{\mathrm{f}} - d_{\mathrm{f},m}}{d_{\mathrm{f,max}} - d_{\mathrm{f},m}}$
for $d_{\mathrm{f}} = d_{\mathrm{f,max}}$:
$u_{\max} = u_{\mathrm{w}}$

The streamwise velocity u_{w} at the interface in the wave peak and the local instantaneous film thickness d_{f} are determined using the LIF technique. Thereby u_{w} is approximated with the wave peak velocity c_{w} which in turn is determined from a two point measurement using a cross correlation method reported for example in Al-Sibai [6].

The temperature dependency of the fluorescence shows only a small influence on the signal height of the fluorescence emission. Increasing the temperature results in a slight decrease of the signal. Comparable behavior is shown by the fluorescence indicator Rhodamine 110 which is used by Sakakibara and Adrian [26]. At constant biacetyl concentration the fluorescence emission solely depends on the film thickness. With appropriate calibration of the measuring device this allows for an accurate measurement of the film thickness.

Before carrying out the experiments some preliminary model-based investigations were done to examine the influence of different temperature and velocity distributions on the phosphorescence signal decay.

Sensitivity calculations were performed assuming three different temperature distributions. These have a constant wall temperature and decrease exponentially in direction of the gas-liquid interface to different surface temperatures, see Fig. 4. The falling liquid film is simulated as being non-wavy with a Reynolds number of $Re_{\mathrm{l}} = 157$, the heated plane is inclined by $\varphi = 3°$ with respect to horizon and for the velocity distribution a parabolic Nusselt profile is assumed.

The resulting normalized decay curves of the phosphorescence intensity are shown in Fig. 5, calculated with Eq. (5). The different slopes of the signals resulting from the assumed temperature distributions is apparently caused

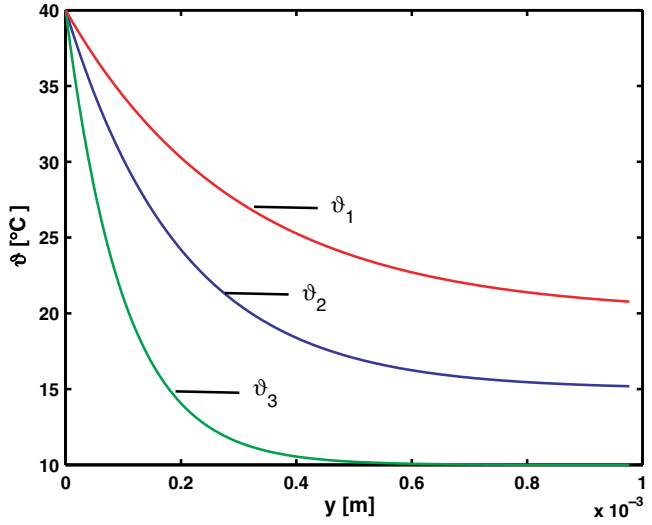

Fig. 4. Assumed temperature profiles for sensitivity investigation.

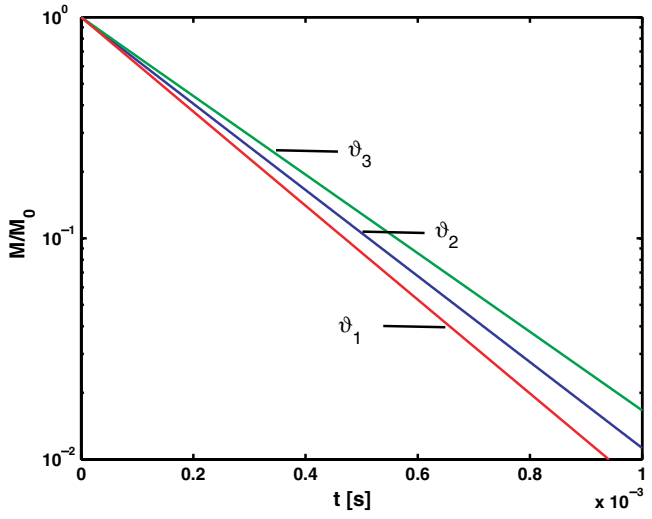

Fig. 5. Sensitivity of phosphorescence decay on different temperature profiles from Fig. 4. For the velocity distribution a parabolic Nusselt profile was assumed (using Eq. (7) and $u_{\max,Nu}$).

by the overall temperature differences varying in the range of 18 K $\leqslant \Delta\vartheta = \vartheta_w - \vartheta_i \leqslant$ 30 K.

The course of the relative deviation between the temperature distribution ϑ_1 and ϑ_2 and between ϑ_3 and ϑ_2 is depicted in Fig. 6. The mean relative deviations are 36% and 32%, respectively. The same is shown for the relative deviations of the resulting signals in Fig. 7. Here the mean relative deviations are 22% and 18%. So a given difference in the temperature distributions results in a difference of the signals with weak information loss.

The influence of different velocity distributions on the phosphorescence decay shows a smaller sensitivity. The signals were calculated, according to Eq. (5), using parabolic velocity distributions with different surface velocities and an exponential temperature profile. The resulting signals for this calculation differ only marginally for short observation times of 1 ms in the simulated measurements and hence are not depicted here. Carrying out the same analysis described above, the mean relative deviations in velocity distribution and resulting signal are 30% and 6%, respectively in both cases. Therefore using an approximative velocity distribution in the evaluation procedure is sufficient as long as the residence time of excited biacetyl molecules within the observation volume is large compared to the measuring time.

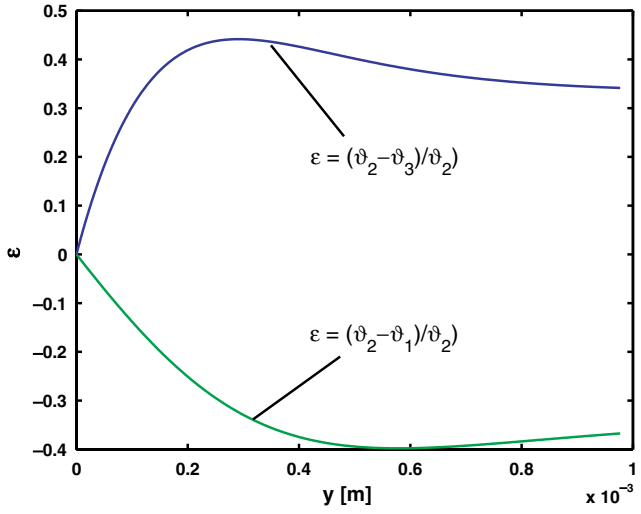

Fig. 6. Relative deviations of the temperature profiles $\vartheta_1(y)$ and $\vartheta_3(y)$ from the temperature distribution $\vartheta_2(y)$.

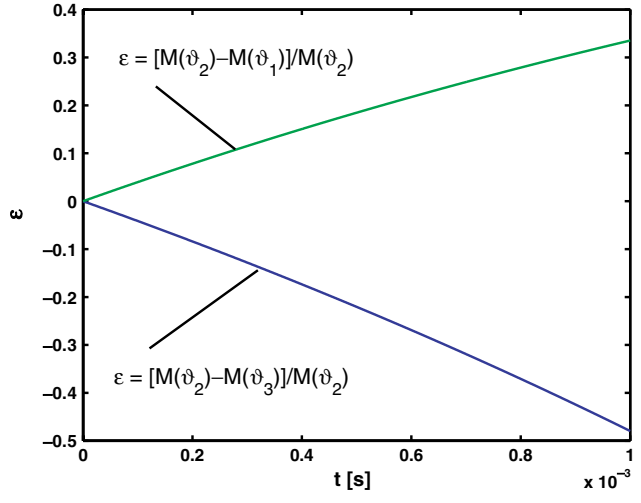

Fig. 7. Relative deviations of the signals M calculated with the temperature profiles $\vartheta_1(y)$ and $\vartheta_3(y)$ from the signal calculated with the temperature distribution $\vartheta_2(y)$.

3. Evaluation method

The objective of the evaluation method is to reconstruct the temperature distribution $\vartheta(y)$ from the measured time dependent optical signal $M(t)$ given by Eq. (5). Such a signal reconstruction is a classical inverse problem, see e.g. Wolfersdorf [30], which in addition is nonlinear and ill-posed. One possibility to solve such a problem is to formulate an optimization task

$$\begin{aligned} &\min_{\vartheta\in\mathbb{R}^n} \quad f(\vartheta) = \min \frac{1}{2}\|M_{\exp}(\vartheta^*) - M(\vartheta)\|_2^2 \\ &\text{s.t.} \quad \vartheta_l \leqslant \vartheta \leqslant \vartheta_u \end{aligned} \tag{8}$$

where $M_{\exp}$ represents the experimental data and M results from a model-based signal calculation using Eq. (5). The constraint restricts the solution ϑ to be within lower and upper bounds. The dimension N is chosen to be 25 for the numerical treatment of the defined optimization task. This is a compromise between computational cost and dependency of the signal on grid resolution in the y-coordinate as well as an implicit regularization to the evaluation of noised data.

The numerical procedure makes use of an evolutionary algorithm, which applies the principles of biological evolution, mutation and selection, to technical systems, see Rechenberg [21] and Schwefel et al. [25,28]. The basics of evolutionary algorithms are described in these books extensively. A flowchart of the iterative procedure to reconstruct the temperature distribution from the measured phosphorescence data is given in Fig. 8.

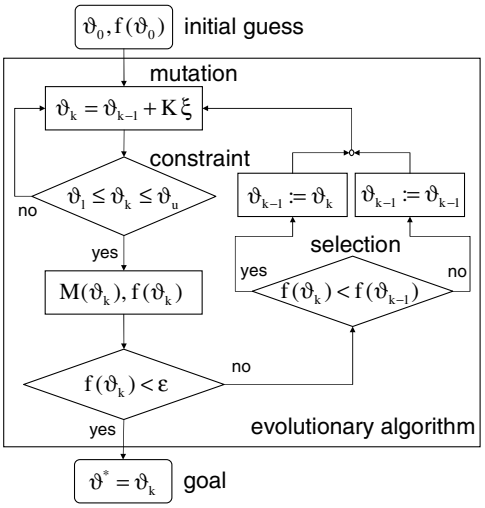

Fig. 8. Model-based method of temperature profile reconstruction using an evolutionary strategy.

Starting with an initial guess of the temperature distribution ϑ_0, the intensity decay of phosphorescence emission $M(\vartheta_0)$ is calculated using Eq. (5). Then a value of the objective function $f(\vartheta_0)$ resulting from comparison of measured signal and calculated signal according to the least-squares problem formulated in Eq. (8) is determined. The mutation step is a random oriented variation of the initial guess to get the next estimation of the temperature distribution $\vartheta_{k=1}$, see Fig. 8. Here ξ are normally distributed random numbers and K is for a simple case a matrix containing the maximal interval in which one component of ϑ can be changed in one mutation step. If the estimate $\vartheta_{k=1}$ satisfies the constraint the signal $M(\vartheta_{k=1})$ and the value of the objective function $f(\vartheta_{k=1})$ are calculated, otherwise the mutation step is restarted. When the objective value is smaller than a given bound the estimated temperature distribution is a good approximation of the real temperature distribution ϑ^*. Otherwise a selection step is applied to check whether the new objective value $f(\vartheta_k)$ is smaller than the old objective value $f(\vartheta_{k-1})$. The temperature distribution related to the smaller value f is used as the starting point of a new cycle of the iterative procedure.

The convergence of the evaluation method to reconstruct the temperature distribution from a phosphorescence decay signal was tested. The results are shown in Figs. 9 and 10.

The residual norm of the given simulated signal and the signal resulting from the reconstruction is 2.5×10^{-12}. The underlying reconstructed temperature distribution fits the given temperature profile with good accuracy. It was shown that even for a stochastically noised signal the temperature distribution can be determined with reasonable accuracy.

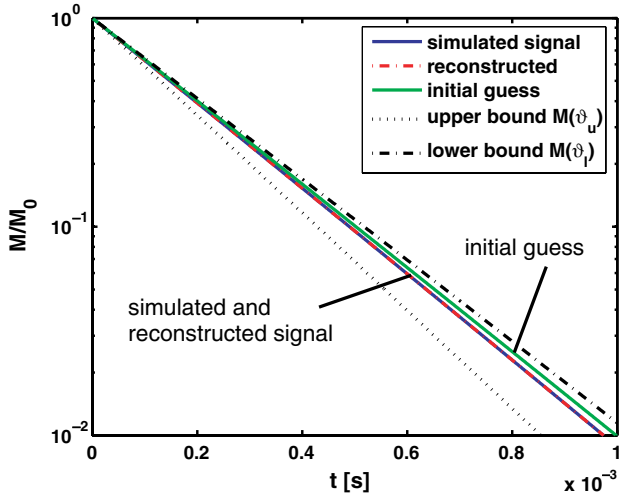

Fig. 9. Signals calculated with the temperature distributions "goal", "initial guess", "lower" and "upper bound", see Fig. 10, and reconstructed signal calculated with the "estimate".

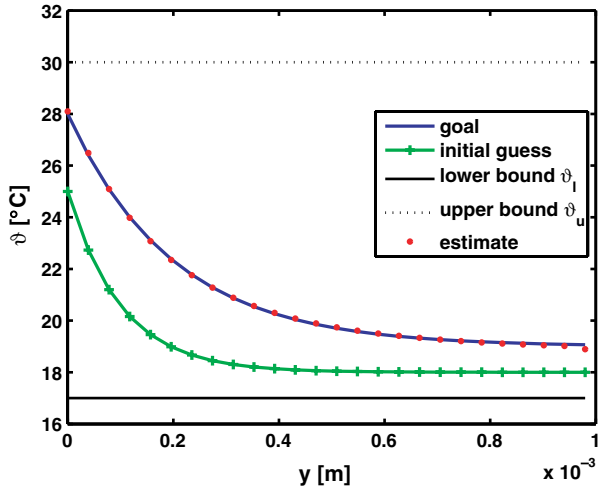

Fig. 10. Reconstruction of the given temperature distribution "goal" by an "estimate" starting from an "initial guess".

4. Experimental design

4.1. Optical measuring technique

The measuring device is basically a phosphoroscope. The source of the primary UV laser beam at a peak wave length of 405 nm is a nitrogen pumped dye laser with a maximum pulse frequency of 50 Hz. As laser dye 4,4′-diphenylstilbene (Lambda Physik AG, Germany) is used. The nitrogen laser pulse has an energy of 116 μJ at a pulse width of 700 ps. A beam splitter optic splits the primary beam into two beams that are sent through light conductors to excite probe volumes in the wavy film with a diameter of about 1 mm. The scheme of the measurement design is shown in Fig. 11.

To obtain information on the wave peak velocity u_w which is needed to characterize the wave properties, the measurement has to be performed at two points in film flow direction simultaneously. The emission of the dissolved and homogeneously distributed biacetyl is measured with four photo-multipliers (Hamamatsu Photonics K.K., Japan). Two of the photo-multipliers measure the phosphorescence to get the temperature profile in the liquid film and the other two measure the fluorescence to get the local film thickness. To separate the information containing indicator

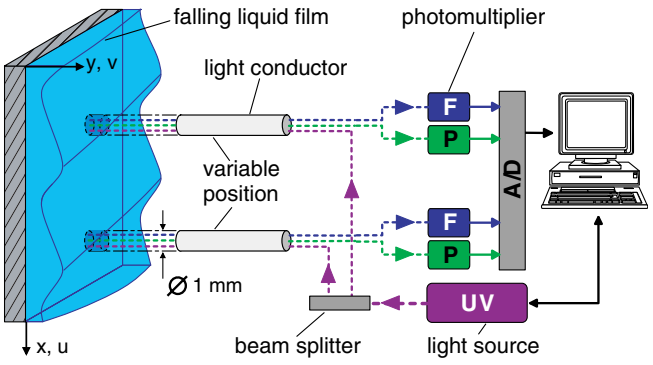

Fig. 11. Principle of simultaneous two point measurement.

emission from the (reflected) excitation light they are equipped with optical edge filters (Schott AG, Germany). For the separation of the phosphorescence edge filters GG 475 and for the separation of fluorescence OG 515 are used. Fig. 12 shows the normalized spectra of excitation and luminescence emission of biacetyl measured with a LIMES-spectrometer (LTB GmbH, Germany).

A spectral separation of fluorescence and phosphorescence is not possible. Here the separation is based on by the different emission lifetimes. The fluorescence has a mean emission lifetime of about 3.6 ns whereas the mean emission lifetime of the phosphorescence is 231 μs in oxygen free water at $\vartheta = 20$ °C. In Fig. 13 the procedure is shown schematically. The fluorescence is measured at the moment of excitation t_0. After a delay time of 1 μs the measurement of the phosphorescence is started at t_1. The corruption of the fluorescence data by phosphorescence can be neglected, because the phosphorescence intensity is two orders of magnitude smaller than the fluorescence intensity in our measurements.

The analog signals of the photo-multipliers are converted to digital signals with a fast A/D-conversion card

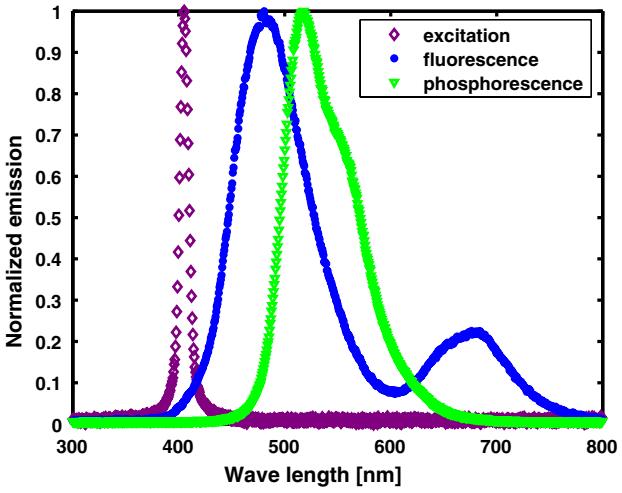

Fig. 12. Normalized emission spectra of excitation, phosphorescence and fluorescence.

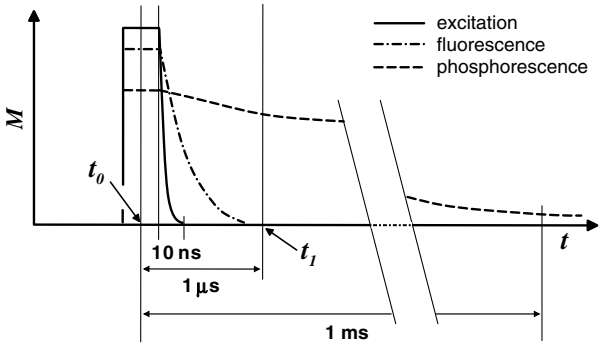

Fig. 13. Scheme of the time dependent behavior of excitation and luminescence emission.

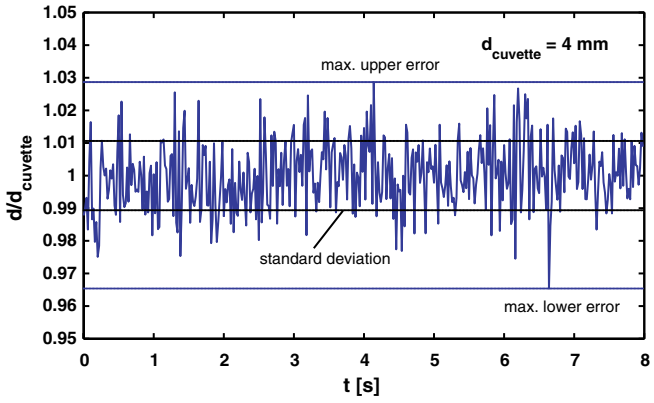

Fig. 14. Standard deviation and maximal error in thickness measurements after correction with simultaneously measured system fluctuations.

(Spectrum GmbH, Germany) with a frequency of 1 MHz per channel so that the temporal resolution of the intensity measurement is 1 μs. The measuring duration after a single laser shot is about 1 ms. The different jitters of the laser and the measuring card were equalized with an external synchronizing clock and a pulse/delay generator (Quantum Composers Inc., USA). The remaining fluctuations in excitation intensity of the laser dye are measured with an additional photo-multiplier. After correction of the indicator emission with the excitation fluctuations, thickness measurements are possible with an accuracy of 1% standard deviation, see Fig. 14. The data within this figure is based on cuvette measurements. A quartz glass cuvette was filled with the same aqueous biacetyl solution as used in the experiments. The maximum deviation in these measurements is 3.5% as indicated in Fig. 14 by the maximum lower error.

Liquid thickness measurements using a petri dish filled to different film heights have shown a linear dependence of fluorescence intensity on liquid film thickness in the range of $d_f = 0.7$–1.4 mm. The distance between the end of the light conductor and the bottom of the petri dish was 4 mm. This is the same distance as in the falling film experiments between the light conductors and the bottom plate of the evaporator. Assuming the same linearity in the falling film experiments the fluorescence measurements are evaluated on the basis of the determined dependance on d_f. According to the thickness measurement at the petri dish the error in film thickness is 2.1% standard deviation in respect to the mean value of 1 mm film thickness.

With the specified measuring device it is possible to simultaneously obtain information about film thickness and temperature distribution every 20 ms. The phosphorescence signal which is used to reconstruct the temperature distribution has a temporal resolution of 1 μs.

4.2. Falling liquid film setup

The experimental setup for the temperature distribution measurement in a falling liquid film is shown schematically in Fig. 15. The main reservoir contains demineralized water

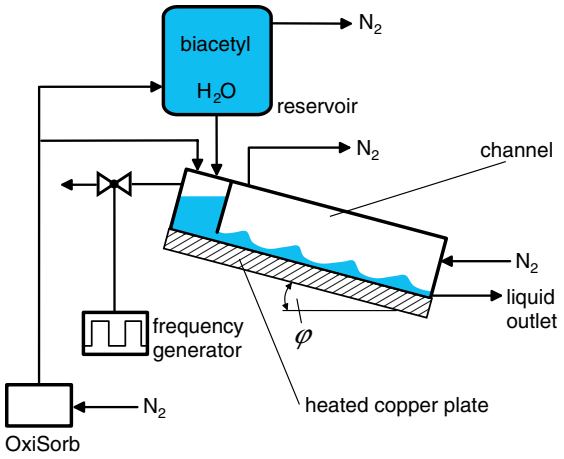

Fig. 15. Scheme of the experimental setup.

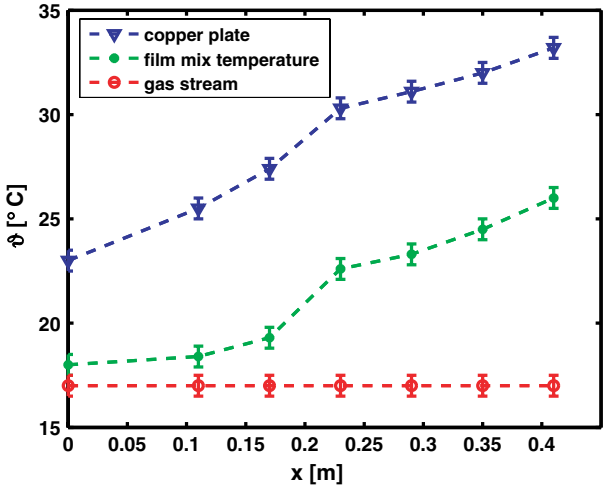

Fig. 16. Surface temperature of the copper plate, mean film temperature and gas stream temperature during the experiment.

degassed with purified nitrogen 5.0. OxiSorb® (Messer-Griesheim GmbH, Germany) is used to remove traces of moisture, oxygen and hydrocarbons from the nitrogen gas supply. The mechanism is a chemisorption of the impurities with reactive chromium compounds. The dissolved oxygen is stripped from the water by nitrogen bubbles. The oxygen concentration is reduced down to 10^{-6} mol/m^3 which is the lower bound of the indicator sensitivity range for measurement of concentration distributions, see Schagen and Modigell [27]. After degasification the luminescence indicator biacetyl is added in a concentration of 11.4 mol/m^3. In this concentration biacetyl does not change the physical properties of the liquid significantly. A measurement of the surface tension of the aqueous biacetyl solution with a du Nuoy tensiometer results in a value of 72.5×10^{-3} N/m. The surface tension of pure water is 72.75×10^{-3} N/m at 20 °C.

The conditioned liquid flows out of the main reservoir into the film device, which can be inclined relative to the horizontal plane in the range of $\varphi = 0°$–$60°$. The liquid flows out of a storage chamber through a manually adjustable slit into the heating chamber with an overall length of $L = 630$ mm, a width of $W = 70$ mm and a height of $H = 30$ mm. With separate gas streams the storage and the main chamber are rinsed to form a nitrogen atmosphere above the liquid surfaces to prevent additional quenching of the phosphorescence by molecular oxygen. A magnetic valve with an adjustable control frequency is installed at the outlet of the storage chamber stream to excite the liquid in this chamber with pressure pulses. Thus the liquid forms a developing laminar-wavy flow in the evaporator.

The falling liquid film is heated from below using an electrically heated copper plate of 6 mm height, 630 mm length and 130 mm width. The copper plate can be heated up to a maximum temperature of $\vartheta_{w,max} = 60$ °C if no liquid film flows down the plate. During the experiment the temperature of the copper plate increases from 23 °C at the liquid inlet to 33.2 °C at the position $x = 410$ mm as can be seen in Fig. 16. These measurements are used as an initial guess for the wall temperature in the evaluation procedure. An integral temperature of the liquid film was invasively measured with a thermocouple. The physical properties of the liquid are calculated with these temperatures and are assumed to be constant while evaluating the phosphorescence signals. For the evaluation point at $x = 230$ mm the temperature is $\vartheta = 22.6$ °C. The properties of water at this temperature are $\rho = 997.635$ kg/m^3, $c_p = 4.1805$ kJ/(kg K), $\lambda = 0.598$ W/(m K), $\eta = 0.949 \times 10^{-3}$ kg/(ms) and the Prandtl number is 6.66. The values are taken from the CRC Handbook of Chemistry and Physics [13] and were kept constant in the evaluation procedure. The temperature of the counter-current gas stream remained constant at 17 °C. All temperatures were measured with an accuracy of ±0.5 °C (Ahlborn Therm 2250-1).

5. Experimental data and evaluation

The settings used during the experiments on the laminar-wavy liquid film flowing down the inclined and heated plane are summarized in Table 1.

5.1. Film thickness and wave velocity

In Fig. 17 the film thickness versus time obtained from fluorescence measurements at position $x = 230$ mm is

Table 1
Parameters of the experimental setup

Design parameter	Name	Value
Liquid side Reynolds number [–]	Re_l	126
Gas side Reynolds number [–]	Re_g	200
Inclination angle [°]	φ	2
Liquid flow rate [l/h]	$\dot{V}_l$	32
Gas flow rate [l/h]	$\dot{V}_g$	551
Disturbance frequency [Hz]	f_d	2
Initial liquid temperature [°C]	ϑ_0	18
Constant gas temperature [°C]	ϑ_g	17

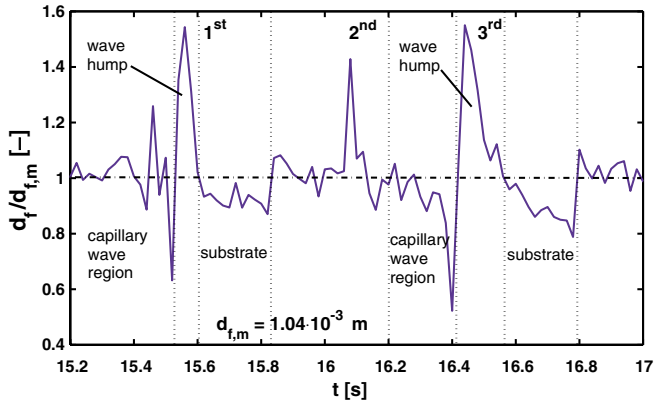

Fig. 17. Film contour at measuring point $x = 230$ mm for $Re = 126$.

depicted. At this position the velocity distribution in flow direction can be approximated with the parabolic profile described by Eq. (7). The mean of fluorescence emission is based on 2000 data points measured in an interval of 40 s. This result constitutes the calibration value that corresponds to the mean film thickness predicted by Nusselt theory [19]

$$d_{f,m} = \left(\frac{3\nu^2 Re_l}{g \sin\varphi}\right)^{1/3} = 1.04 \times 10^{-3}\ \text{m}. \tag{9}$$

Experimental values of Brauer [9] for vertical films and Al-Sibai [6] for inclined wavy films confirm the relation of Nusselt for the film thickness.

In Fig. 17 the course of the film thickness over time is depicted relative to the mean film thickness. Looking at the first and the third wave three characteristic regions of a single wave can be identified. The capillary wave region in front of the wave hump, which consists of the wave crest and the wave back, and the substrate behind the wave back. The maximum height of the wave peaks with respect to the mean film thickness is about 55%. The minimal film thickness with respect to the mean film thickness of about 40% is located in front of the wave hump.

Analyzing the fluorescence data leads to the mean wave length $\lambda_w = 0.18$ m and the mean wave velocity $u_w = 0.4$ m/s. From a Fourier analysis the primary wave frequency can be determined as $f_w = 2$ Hz which corresponds to the excitation frequency. Higher order frequencies which can be found in the power spectrum result from the capillary waves in front of the main wave.

The film surface contour at the measuring point is not exactly periodic and equal in shape. One reason is that in the laminar-wavy liquid flow the waves are not fully developed hydrodynamically at the measuring point. This is in accordance with results of Ramaswamy et al. [20] who showed in direct numerical simulations that with increasing Reynolds number the length of the wave developing region increases too. Already at a Reynolds number of $Re_l = 60$ and an inclination angle $\varphi = 6.4°$ the wave developing region reaches a length of 0.4 m.

5.2. Temperature distributions

The temperature distribution is obtained from the decay of phosphorescence intensity. Such a phosphorescence intensity decay curve is measured with a temporal resolution of 1 μs. For the reconstruction of a temperature profile the phosphorescence decay within ≈0.6 ms is used. The spatial resolution depends on the number of points to which the temperature distribution is numerically mapped in the evaluation procedure ($N = 25$). Therefore the spatial resolution is about 40 μm in y-direction.

In this section the results for the temperature distributions for the third wave of Fig. 17 are presented. The evaluation of the signal measured in the wave peak is described exemplarily. In Fig. 18 the noisy phosphorescence signal measured within the wave peak at $t = 16.44$ s is given. With the upper and lower temperature bounds, see Fig. 19, the

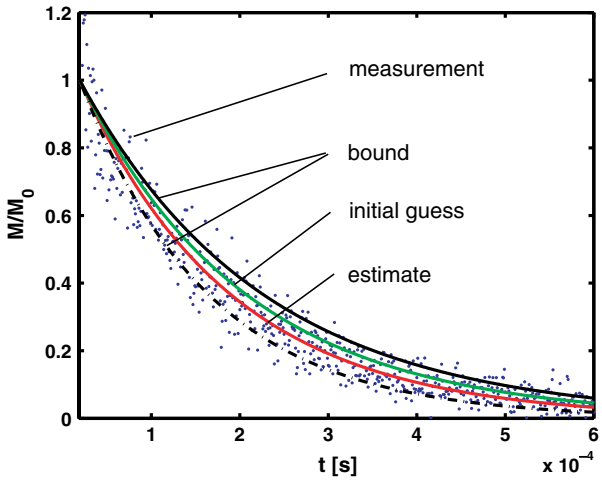

Fig. 18. Phosphorescence decay curve measured in the peak of the third wave of Fig. 17. Model-based signals calculated with temperature bounds, the initial guess for the temperature distribution and with the estimated temperature distribution, see Fig. 19.

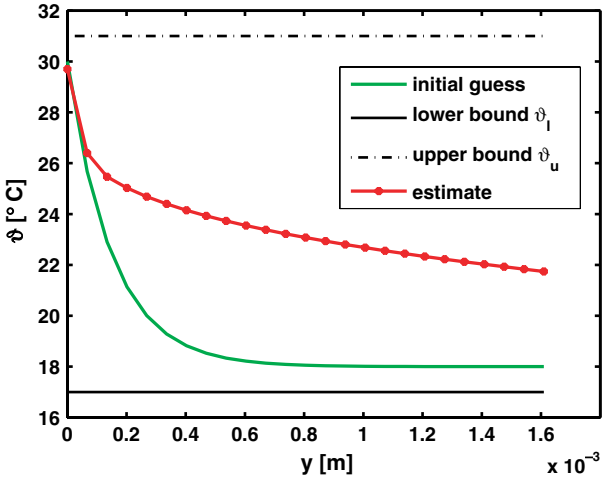

Fig. 19. Temperature constraints to restrict the solution space, initial guess and reconstructed temperature distribution from evaluation of the measured signal shown in Fig. 18.

region of possible solutions is confined. The resulting model-based signals are depicted in Fig. 18. The initial guess for the temperature distribution makes use of the wall temperature of $\vartheta_w = 30\,°C$ at the position $x = 230\,mm$ and the liquid inlet temperature, see Fig. 16. Although the initial guess is generated with an exponential model, this model was not used for evaluation. The estimated temperature profile shows a steep gradient at the wall and a non-vanishing gradient at the interface.

To confirm that the reconstructed temperature profile is an accurate fit to the experimental data, the mean relative deviations ε of the data from the calculated signals were determined according to

$$\varepsilon_{i,m} = \frac{1}{k}\sum_{j=1}^{k}\frac{M_i(t_j) - M_{exp}(t_j)}{M_i(t_j)} \tag{10}$$

with $i = 1$: estimate, 2: initial guess, 3: upper bound, 4: lower bound.

Fig. 20 shows the relative deviations $\varepsilon_1(t)$ of the experimental data from the signal calculated with the estimate of the temperature distribution and the corresponding mean value $\varepsilon_{1,m} = -0.0097$. Further the mean relative deviations of the experimental data from the remaining signals were calculated. The mean relative deviations are $\varepsilon_{2,m} = 0.0946$ with respect to the initial guess, $\varepsilon_{3,m} = -0.362$ with respect to the upper bound (ϑ_u) and $\varepsilon_{4,m} = 0.159$ with respect to the lower bound (ϑ_l). Evidently the mean relative deviation $\varepsilon_{1,m}$ is one order of magnitude closer to zero than the value with respect to the initial guess $\varepsilon_{2,m}$. Thus the estimated temperature profile gives the best phosphorescence signal to fit the measured data.

Evaluation of all phosphorescence signals obtained from the third wave in Fig. 17 leads to the temperature field shown in Fig. 21. It can be seen that the surface temperature as well as the temperature gradients in y-direction differ along the wave. In the wave crest and the wave back the temperature gradient is steeper than in the capillary wave region. The maximum change in the gradient along the wave can be localized in front of the wave peak. The wave hump, in which a large amount of mass with lower temperature is transported, flattens the temperature boundary layer of the substrate. The surface temperature in the wave crest and the wave back varies from 21.7 to 23 °C. In the capillary wave region a nearly constant temperature of 24 °C is reached.

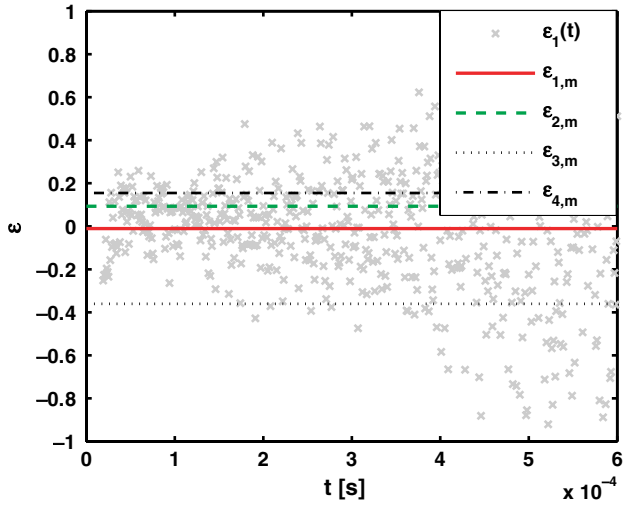

Fig. 20. Relative deviations ($\varepsilon_1(t)$) of the experimental data from the signal calculated with the reconstructed temperature distribution. The corresponding mean value ($\varepsilon_{1,m}$) is compared to the mean values of the relative deviations of the initial guess ($\varepsilon_{2,m}$) and the bounds ($\varepsilon_{3,m}$, $\varepsilon_{4,m}$).

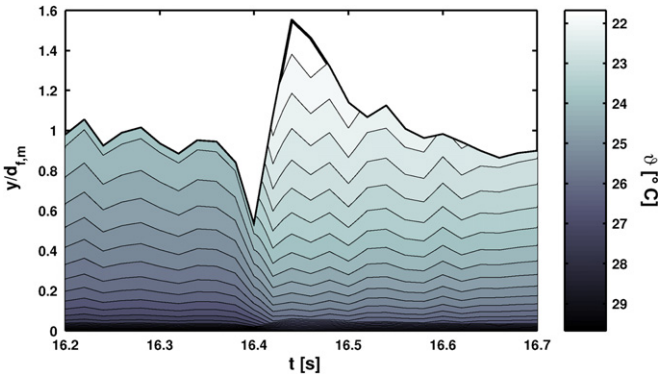

Fig. 21. Iso temperature lines along the wave at position $x = 230\,mm$ for $Re = 126$.

6. Investigation of heat transfer in the wavy film flow

6.1. Local instantaneous heat transfer coefficient

In investigations on heat transfer in falling liquid film evaporators or reactors often a constant local heat transfer coefficient is assumed. As a result of the proposed measurement method it can be shown that this assumption is a simplification especially in the case of a wavy film.

The local heat transfer coefficient for the considered case is defined as

$$\alpha_{w,i} = -\frac{\lambda\frac{\partial\vartheta}{\partial y}\big|_{y=0,d_f}}{\Delta\vartheta_{w,i}} \tag{11}$$

with the indices w and i denoting the wall and the interface respectively. Heat transfer is driven by the overall temperature difference, which is in the case of transfer from the wall to the liquid is defined as $\Delta\vartheta_w = \vartheta_w - \vartheta_i$. Looking at the transport from the liquid to the gas phase it is $\Delta\vartheta_{\,i} = \vartheta_i - \vartheta_g$, the latter being the gas temperature. In Fig. 22 the course of the local heat transfer coefficient is depicted for both cases normalized to the respective mean value.

The mean transfer coefficient at the heated wall is determined as $\alpha_{w,m} = 2190.5\,W/(m^2\,K)$ and for the value at the interface $\alpha_{i,m} = 184.2\,W/(m^2\,K)$ is obtained. Both curves of the local heat transfer coefficient show a significantly higher value in front of the wave and a minimum beneath the wave hump. After that the curves increase slowly to their mean values. This is in qualitative agreement with

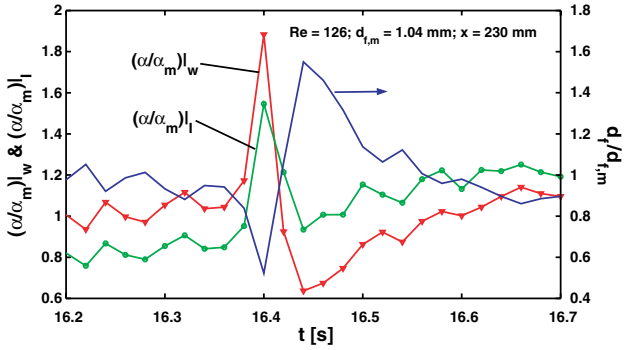

Fig. 22. Local heat transfer coefficient along the wave at position $x = 230$ mm.

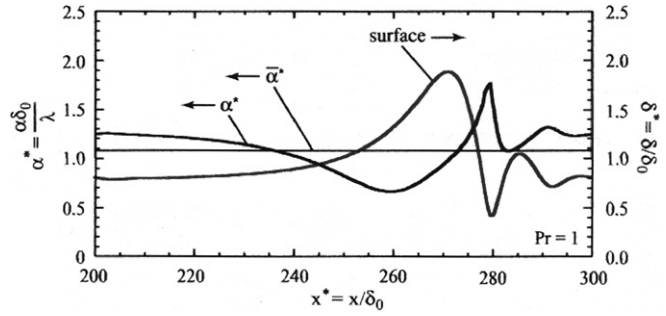

Fig. 23. Wave surface and instantaneous dimensionless local heat transfer coefficient α^* at $Re = 50$, taken from Adomeit et al. [1].

the experimental results of Al-Sibai et al. [8]. The peak of the transfer coefficients in front of the wave as a result of our experiments cannot be found in their experiments. Possibly it is caused by the different experimental setups. Al-Sibai et al. used an electrically heated thin foil (2 μm) to realize a constant heat flux into a silicon oil film excited with 10 Hz to laminar-wavy flow, a Reynolds number of 14.5 and a Prandtl number of 10. Numerical simulations of Adomeit et al. [1] for a Reynolds number of 50 and a Prandtl number of 1 are in good agreement with our experimental results, see Fig. 23. The course of the dimensionless local heat transfer coefficient is qualitatively the same. Especially the peak in front of the wave and the behavior beneath the wave is congruent.

6.2. Quantification of wave-induced convective heat transfer

It is well established, that different mechanisms lead to an increase in local heat transfer observed in wavy film flow. On one hand thinning of the residual layer due to wave propagation leads to a reduced conductive resistance. On the other hand wave-induced convective transport perpendicular to the bounding wall results in the exchange of fluid between the region near the interface and the region near the wall, which in turn leads to a local increase in the slope of the temperature field. DNS data, obtained by Miyara [17] for heat transfer in evaporating wavy film flow, shows that the former mechanism predominates at low values of the Prandtl number, while the later is prevalent at high values of the Prandtl number.

In the present work the experimental data presented in the previous sections where used to investigate the wave-induced convective heat transfer inside the wavy film flow. therefore the convective heat flux perpendicular to the wall was quantified with the goal of identifying the regions of a representative wave which predominantly contribute to this mode of transport. For the quantitative evaluation the concept of an effective heat flux subsuming diffusional and convective heat transfer was employed.

Heat transfer in the wavy film flow is governed by the unsteady energy equation without source terms:

$$\frac{\partial \vartheta}{\partial t} + u \cdot \frac{\partial \vartheta}{\partial x} = \kappa \cdot \frac{\partial^2 \vartheta}{\partial x^2} + \underbrace{\kappa \cdot \frac{\partial^2 \vartheta}{\partial y^2} - v \cdot \frac{\partial \vartheta}{\partial y}}_{F} \tag{12}$$

In order to quantify the effect of convective heat transfer perpendicular to the wall all terms describing heat transfer in y-direction are subsumed in the generalized flux F. Arbitrarily the generalized flux is formulated as a generalized diffusional term in y-direction introducing an effective heat flux $\dot{q}''_{\mathrm{eff}}$

$$F \equiv -\frac{1}{\rho \cdot c} \cdot \frac{\partial \dot{q}''_{\mathrm{eff}}}{\partial y} \tag{13}$$

which thereby constitutes a parameter quantifying the sum of the convective and diffusional heat fluxes in y-direction. A definition for $\dot{q}''_{\mathrm{eff}}$ can be obtained by integrating the generalized flux F in y-direction having introduced Eq. (13)

$$\dot{q}''_{\mathrm{eff}} = \dot{q}''_{\mathrm{eff}}|_{y=d_{\mathrm{f}}} + \rho \cdot c \cdot \int_{y}^{d_{\mathrm{f}}} \left(\kappa \cdot \frac{\partial^2 \vartheta}{\partial y^2} - \mathrm{v} \cdot \frac{\partial \vartheta}{\partial y} \right) \mathrm{d}y \tag{14}$$

Due to the fact that Eq. (13), defining the effective heat flux, is a first order differential equation the definition of $\dot{q}''_{\mathrm{eff}}$ contains the boundary value $\dot{q}''_{\mathrm{eff}}|_{y=d_{\mathrm{f}}}$. In the absence of a plausible boundary condition for $\dot{q}''_{\mathrm{eff}}$ at the interface this quantity cannot be determined. To adequately quantify the effect of wave-induced convective heat transfer it must therefore be eliminated.

This can be achieved by introducing the relative quantity γ:

$$\gamma = \frac{(\dot{q}''_{\mathrm{eff}} - \dot{q}''_{\mathrm{eff}}|_{y=d_{\mathrm{f}}})}{\dot{q}''_{\mathrm{diff}}} \tag{15}$$

Here $\dot{q}''_{\mathrm{diff}}$ designates the local, instantaneous diffusional heat flux in y-direction defined by Fourier's law

$$\dot{q}''_{\mathrm{diff}} = -\lambda \cdot \frac{\partial \vartheta}{\partial y} \tag{16}$$

Neglecting the diffusional heat transfer in y-direction at the interface the parameter γ can be interpreted as the ratio of the difference of the effective and diffusional heat fluxes between the considered point and the interface. It thereby enables a quantitative assessment of the relative significance of the wave-induced convective heat transfer.

Insertion of Eq. (14) into Eq. (15) yields:

$$\gamma = \frac{\rho \cdot c \cdot \int_y^{d_f} \left(\kappa \cdot \frac{\partial^2 \vartheta}{\partial y^2} - v \cdot \frac{\partial \vartheta}{\partial y} \right) dy}{\dot{q}''_{diff}} \tag{17}$$

Thus γ can be determined on the basis of the experimental data described in this work using Eq. (17).

The terms $\frac{\partial \vartheta}{\partial y}$ and $\frac{\partial^2 \vartheta}{\partial y^2}$ can be directly calculated from the experimental data. The component v of the velocity vector has to be approximated and shall be addressed here. Assuming the approximated distribution of the component u of the velocity vector introduced in Section 2 the component v follows from the continuity equation for an incompressible fluid

$$v = -\int_0^y \left(\left. \frac{\partial u}{\partial x} \right|_y \right) dy \tag{18}$$

More considerable difficulties arise regarding the evaluation of the differential $\frac{\partial u}{\partial x}|_y$. No information with respect to variation in x-direction is obtainable directly from the experiment. However current efforts concentrate on temperature and film thickness measurements with higher spatial resolution in x-direction. For the time being an approximation of $\frac{\partial u}{\partial x}|_y$ has to suffice.

Introducing some simplifications the partial derivative $\frac{\partial u}{\partial x}|_y$ can be approximated as follows:

$$\left. \frac{\partial u}{\partial x} \right|_y = -\frac{1}{c_w} \cdot \frac{\partial u^*}{\partial t} + \frac{\partial u}{\partial y} \cdot \frac{\partial d_f}{\partial t} \cdot \frac{1}{c_w} \cdot \frac{y}{d_f} \tag{19}$$

A detailed description of the derivation of the above equation is presented in Appendix.

Fig. 24 depicts three curves of the parameter γ for different times of the temporal development of the representative solitary wave pictured in Fig. 21. The different curves are associated with the respective wave regions classified in Fig. 17. The depicted results show, that the relative significance of the convective heat flux in y-direction as quantified by the parameter γ reaches a maximum in the region of the center of the liquid layer at all considered points in time. Further it is discernible, that the maximum value of γ is greatest for the point in time associated with the development of the wave crest. The distributions of γ associated with the capillary wave region and the substrate region respectively exhibit considerably smaller values.

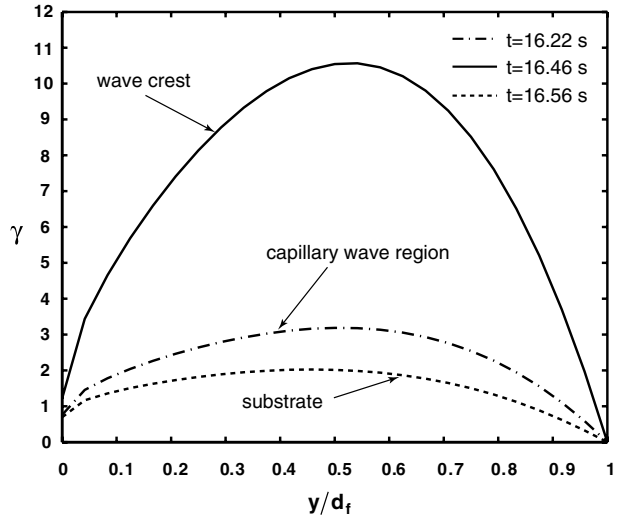

Fig. 24. γ as a function of wall distance for three times in the temporal development of a representative wave pictured in Fig. 21.

7. Conclusion

A new measurement method for the determination of the temperature distribution with high spatial and temporal resolution in thin liquid films is presented. This method is based on the temperature dependent emission lifetime of an optical indicator. First results for the heat transport in a wavy falling liquid film flowing down a heated plane are presented exemplarily.

With the temperature profiles determined from measurements in a laminar-wavy falling liquid film the local heat transfer coefficients and a parameter quantifying the relative significance of convective heat transfer perpendicular to the wall at three points in the development of a solitary wave are calculated. The calculations show that the local heat transfer coefficient is not constant along the wave as it is often assumed. Here the maximum value is reached in front of the wave between the capillary wave region and the wave crest. The results also indicate a wave induced intensification of heat transfer due to convective transport perpendicular to the wall in the central region of the film.

Further investigations of the kinetic phenomena covering single waves will be done for laminar-wavy falling liquid films flowing down a heated plane at different positions in flow direction varying Reynolds number and inclination angle of the evaporator. The results will be the basis for research of coupled heat and mass transfer mechanisms including chemical reactions in falling liquid films.

Acknowledgements

The authors gratefully acknowledge the financial support of the Deutsche Forschungsgemeinschaft (DFG) within the Collaborative Research Center (SFB) 540 "Model-based Experimental Analysis of Kinetic Phenomena in Fluid Multi-phase Reactive Systems".

Appendix. Approximation of the streamwise derivative of *u*

To determine the approximation for $\frac{\partial u}{\partial x}|_y$, the field of the velocity component u is mapped from the temporally variable domain constituted by the liquid phase to a domain which is temporally invariant:

$$u(x, y, t) \mapsto u^*(x, \xi, t)$$

$$\xi = \frac{y}{d_f(x, t)}$$

It can be generally stated, that the field of the film thickness and as a consequence the mapped field of the velocity component u^* are periodic with respect to the coordinates t and x. Thus u^* can be formulated as:

$$u^*(x,\xi,t) = \overline{u^*}(\xi) + \Psi(\eta,\xi) \tag{20}$$

with:

$$\eta = \omega \cdot t - k \cdot x$$

$$\Psi = \sum_{i=1}^{\infty} a_i(\xi) \cdot \cos(i \cdot \eta) + \sum_{i=1}^{\infty} b_i(\xi) \cdot \sin(i \cdot \eta)$$

It was thereby assumed, that the amplitude of the oscillation of the film thickness and consequently of the velocity component u^* is independent of η.

The partial derivative $\frac{\partial u^*}{\partial x}|_\xi$ of the mapped field of the velocity component in x-direction thus follows:

$$\left.\frac{\partial u^*}{\partial x}\right|_\xi = -\frac{1}{c_w} \cdot \frac{\partial u^*}{\partial t} \tag{21}$$

The partial derivative $\frac{\partial u}{\partial x}|_y$ then results from $\frac{\partial u^*}{\partial x}|_\xi$ by backward transformation

$$\left.\frac{\partial u}{\partial x}\right|_y = \left.\frac{\partial u^*}{\partial x}\right|_\xi - \frac{\partial u}{\partial y} \cdot \frac{\partial d_f}{\partial x} \cdot \xi \tag{22}$$

Finally following the same procedure as elaborated above the spatial derivative of the film thickness can be expressed as a function of the corresponding temporal derivative under the introduced assumptions:

$$\frac{\partial d_f}{\partial x} = -\frac{\partial d_f}{\partial t} \cdot \frac{1}{c_w} \tag{23}$$

yielding the following expression for the approximative quantification of the partial derivative $\frac{\partial u}{\partial x}|_y$:

$$\left.\frac{\partial u}{\partial x}\right|_y = -\frac{1}{c_w} \cdot \frac{\partial u^*}{\partial t} + \frac{\partial u}{\partial y} \cdot \frac{\partial d_f}{\partial t} \cdot \frac{1}{c_w} \cdot \frac{y}{d_f} \tag{24}$$

References

[1] P. Adomeit, A. Leefken, U. Renz, Experimental and numerical investigations on wavy films, in: Proceedings of the 3rd European Thermal Science Conference, vol. 2, 2000, pp. 1003–1009.

[2] K. Alhusseini, M. Tuzla, J.C. Chen, Falling film evaporation of single component liquids, Int. J. Heat Mass Transfer 41 (1998) 1623–1632.

[3] S.V. Alekseenko, V.E. Nakoryakov, P.G. Pokusaev, Wave effect on the transfer processes in liquid films, Chem. Eng. Comm. 141 (1996) 359–385.

[4] S.V. Alekseenko, V.E. Nakoryakov, P.G. Pokusaev, Wave flow of liquid films, Begell House, New York, 1994.

[5] M. Almgren, The natural phosphorescence lifetime of biacetyl and benzyl in fluid solution, Photochem. Photobiol. 6 (1968) 829–840.

[6] F. Al-Sibai, Local and instantaneous distribution of heat transfer rates and velocities in thin wavy films, Ph.D. thesis, RWTH Aachen, Aachen, 2005.

[7] F. Al-Sibai, A. Leefken, U. Renz, Local and instantaneous distribution of heat transfer rates and velocities in thin wavy films, in: Proceedings of Eurotherm 71 on Visualization, Imaging and Data Analysis in Convective Heat and Mass Transfer, Reims, France, October 2002, pp. 28–30.

[8] F. Al-Sibai, A. Leefken, U. Renz, Local and instantaneous distribution of heat transfer rates through wavy films, Int. J. Thermal Sci. 41 (7) (2002) 658–663.

[9] H. Brauer, Grundlagen der Einphasen- und Mehrphasenströmungen, Verlag Sauerländer, Aarau und Frankfurt am Main, 1961, pp. 673.

[10] N. Brauner, D.M. Maron, Characteristics of inclined thin films, waviness and the associated mass transfer, Int. J. Heat Mass Transfer 25 (1) (1982) 99–110.

[11] H.L.J. Bäckström, K. Sandros, The quenching of the long-lived fluorescence of biacetyl in solutions, Acta Chem. Scand. 12 (1958) 823–832.

[12] A.T. Conlisk, Analytical solutions for the heat and mass transfer in a falling film absorber, Chem. Eng. Sci. 50 (4) (1995) 651–660.

[13] D.R. Lide (Ed.), CRC Handbook of Chemistry and Physics, 80th ed., CRC Press LLC, Boca Reaton, 2000.

[14] K. Hishida, J. Sakakibara, Combined planar laser-induced fluorescence-particle image velocimetry technique for velocity and temperature fields, Exp. Fluids 29 (2000) 129–141.

[15] J.D. Killion, S. Garimella, A critical review of models of coupled heat and mass transfer in falling-film absorption, Int. J. Refrig. 24 (2001) 755–797.

[16] V.V. Lel, A. Leefken, F. Al-Sibai, U. Renz, Extension of the chromatic confocal imaging method for local thickness measurements of wavy films, in: Proceedings of 5th International Conference on Multiphase Flow, ICMF'04, Yokohama, Japan, May 30–June 4 2004, 20 Paper No. 155.

[17] A. Miyara, Numerical analysis on flow dynamics and heat transfer of falling liquid films with interfacial waves, Heat Mass Transfer 35 (1999) 298–306.

[18] S. Miladinova, S. Slavtchev, G. Lebon, J.C. Legros, Long-wave instabilities of non-uniformly heated falling films, J. Fluid Mech. 453 (2002) 153–175.

[19] W. Nusselt, Die Oberflächenkondensation des Wasserdampfes, Z. VDI 60 (1916) 514–546.

[20] B. Ramaswamy, S. Chippada, S.W. Joo, A full-scale numerical study of interfacial instabilities in thin-film flow, J. Fluid Mech. 325 (1996) 163–194.

[21] I. Rechenberg, Evolutionsstrategie '94 – Werkstatt Bionik und Evolutionstechnik, Frommann–Holzboog, Stuttgart, 1994.

[22] R.M. Roberts, H.C. Chang, Wave-enhanced interfacial transfer, Chem. Eng. Sci. 55 (2000) 1127–1141.

[23] A. Günther, P. Rudolf von Rohr, Simultaneous visualization of temperature and velocity fields in turbulent natural convection, in: Proceedings of the 34th National Heat Transfer Conference, Pittsburgh, 2000.

[24] A. Günther, P. Rudolf von Rohr, Influence of the optical configuration on temperature measurements with fluid-dispersed TLCs, Exp. Fluids 32 (2002) 533–541.

[25] G. Rudolph, H.P. Schwefel, Evolutionäre Algorithmen – ein robustes Optimierkonzept, Phys. Blätter, Weinheim 50 (3) (1994) 236–238.

[26] J. Sakakibara, R.J. Adrian, Whole field measurement of temperature in water using two-color laser induced fluorescence, Exp. Fluids 26 (1999) 7–15.

[27] A. Schagen, M. Modigell, Luminescence technique for the measurement of local concentration distribution in thin liquid films, Exp. Fluids 38 (2005) 174–184.

[28] H.P. Schwefel, Evolution and Optimum Seeking Sixth-Generation Computer Technology Series, Wiley, Interscience, 1995.

[29] F.K. Wasden, A.E. Dukler, A numerical study of mass transfer in free falling films, AIChE J. 36 (1990) 1379–1390.

[30] L. Wolfersdorf, Inverse und schlecht gestellte Probleme – Eine Einführung, Sitzung. sächsischen Akad. Wissen. Leipzig 124 (5) (1994).